

# Virtual sensors for active noise control in acoustic-structural coupled enclosures using structural sensing: Part II—Optimization of structural sensor placement

Dunant Halim, Li Cheng,<sup>a)</sup> and Zhongqing Su

Department of Mechanical Engineering, The Hong Kong Polytechnic University, Kowloon, Hong Kong

(Received 20 October 2010; revised 4 January 2011; accepted 5 January 2011)

The work proposed an optimization approach for structural sensor placement to improve the performance of vibro-acoustic virtual sensor for active noise control applications. The vibro-acoustic virtual sensor was designed to estimate the interior sound pressure of an acoustic-structural coupled enclosure using structural sensors. A spectral-spatial performance metric was proposed, which was used to quantify the averaged structural sensor output energy of a vibro-acoustic system excited by a spatially varying point source. It was shown that (i) the overall virtual sensing error energy was contributed additively by *the modal virtual sensing error* and the measurement noise energy; (ii) each of the modal virtual sensing error system was contributed by both the modal observability levels for the structural sensing and the target acoustic virtual sensing; and further (iii) the strength of each modal observability level was influenced by the modal coupling and resonance frequencies of the associated uncoupled structural/cavity modes. An optimal design of structural sensor placement was proposed to achieve sufficiently high modal observability levels for certain important panel- and cavity-controlled modes. Numerical analysis on a panel-cavity system demonstrated the importance of structural sensor placement on virtual sensing and active noise control performance, particularly for cavity-controlled modes. © 2011 Acoustical Society of America. [DOI: 10.1121/1.3552873]

PACS number(s): 43.55.Jz, 43.60.Bf, 43.40.Rj [NX]

Pages: 1991–2004

## I. INTRODUCTION

In controlling the interior sound field of an enclosure, an active local control strategy can be used together with *error sensors* located at a certain location to create a *zone of quiet*, in which the noise level is considerably reduced. The error sensors can be microphones or other acoustic sensors which measure local acoustic quantities to be minimized by active control algorithms (Elliott, 2001). In practice, it may not always be possible or convenient to place sensors at the target location for noise control. In this case, the active control strategy can utilize an *acoustic virtual sensor*, whose purpose is to estimate local acoustic quantities using real/physical acoustic sensors at a remote location.

Moreau *et al.* (2008) reviewed various acoustic virtual sensing methods that were proposed by a number of researchers, e.g., *the virtual microphone technique* (Elliott and David, 1992), *the remote microphone technique* (Popovich, 1997; Roure and Albarrazin, 1999), *the forward difference prediction and adaptive LMS techniques* (Cazzolato, 1999, 2002), *the Kalman filtering technique* (Petersen *et al.*, 2008), and *the virtual sensing technique for a diffused sound field* (Moreau *et al.*, 2009). A number of theoretical and experimental studies, such as for active headrest applications (e.g., Rafaely *et al.*, 1999; Pawelczyk, 2003), have demonstrated successful active control implementations for creating a *zone of quiet* at the virtual sensor location.

Such an *acoustic virtual sensor* can be used for active control of interior sound field of an acoustic-structural coupled enclosure. However, albeit at different locations, real/physical acoustic sensors are still needed to be placed within the enclosure. The possibly large sensors and their wiring may be detrimental to the esthetics of the interior. In contrast, compact structural sensors, attached to flexible sides or panels, can be used as a *virtual sensor* which keeps the interior “clean” from sensors and wiring. For this purpose, a *vibro-acoustic virtual sensor* was proposed by Halim *et al.* (2011), which allowed active control of local interior sound field using only structural sensors. This vibro-acoustic virtual sensor is different from spatial or modal filters that use discrete or distributed structural sensors (e.g., Snyder and Tanaka, 1993; Cazzolato, 1999; Smith and Clark, 2001; Hill *et al.*, 2009). Such spatial/modal sensors have potential sensing limitations due to “leakage” because of discrete spatial sampling or imperfections of distributed sensor patterns (Cazzolato, 1999).

Halim *et al.* (2011) pointed out the importance of structural sensor placement for the vibro-acoustic virtual sensing performance. The structural sensor placement is important because the path for sensing the interior sound field, excited by an interior acoustic source, is only through the acoustic-structural coupling (Cheng, 1994). This coupling is generally weak for a practical vibro-acoustic enclosure which consists of relatively stiff panels for load-carrying purposes. If a structural sensor was placed at a location where important cavity-controlled modes were not observed well, the virtual sensing performance would be degraded regardless of how the virtual sensor filter was designed. However, finding the

<sup>a)</sup>Author to whom correspondence should be addressed. Electronic mail: mmlcheng@inet.polyu.edu.hk

“best” structural sensor location for a vibro-acoustic system is not a straightforward process since interactions among multiple vibration and acoustic modes must be taken into account. Such a problem provides the motivation of the current work in structural sensor placement. The aims of the work are thus: (i) to investigate how the structural sensor placement can affect the virtual sensing accuracy; (ii) to propose a systematic framework for optimization of structural sensor placement to improve the virtual sensing and active control performances.

The structure of the paper is organized as follows: Sec. II presents the modal model of an acoustic-structural coupled enclosure, with the focus on a rectangular panel-cavity system. Section III proposes an optimization framework for structural sensor placement with a hope for improving the vibro-acoustic virtual sensor performance. Section IV provides a numerical analysis of structural sensor placement on a coupled panel-cavity system, including its effects on virtual sensing and active control performances. The work is concluded in Sec. V.

## II. MODEL OF VIBRO-ACOUSTIC ENCLOSURES

Here, the dynamic model of vibro-acoustic enclosures with acoustic-structural coupling was considered. As a benchmark, a rectangular panel-cavity system in an  $x$ - $y$ - $z$  Cartesian coordinate system was used as a representative vibro-acoustic system, as shown in Fig. 1. More complex systems can also be incorporated based on modal properties that are estimated from numerical models or experimental system identification methods. For the current configuration, the following partial differential equations apply (Fahy, 1985; Cheng and Nicolas, 1992),

$$\begin{aligned} \nabla^2 p(x, y, z, t) - \frac{1}{c^2} \ddot{p}(x, y, z, t) \\ = -\rho \dot{q} + 2\rho \ddot{w}(x, y, t) \delta(z - z_0), \end{aligned} \quad (1)$$

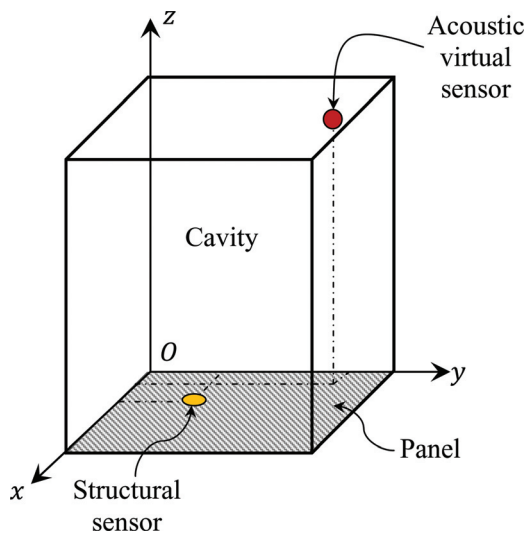


FIG. 1. (Color online) A rectangular panel-cavity system with a structural sensor attached on the flexible panel and an acoustic virtual sensor inside the cavity.

$$\begin{aligned} D \nabla^4 w(x, y, t) + m \ddot{w}(x, y, t) = f(t) \delta(x - x_f) \delta(y - y_f) \\ + p(x, y, z_0, t), \end{aligned} \quad (2)$$

where the flexible panel was located along  $z = z_0$ . Here,  $p$  is the interior sound pressure at location  $(x, y, z)$ ;  $q$  is the acoustic source volume velocity per unit volume;  $w$  is the transverse panel displacement at location  $(x, y)$ ;  $c$  is the speed of sound in the fluid;  $\rho$  is the fluid density;  $m$  is the panel mass per unit area;  $f$  is the external point force applied at location  $(x_f, y_f)$ ;  $\delta(\cdot)$  is the Dirac delta function; and  $D = Ed^3/12(1 - \nu^2)$  is the panel stiffness with  $E$ ,  $d$ , and  $\nu$  being the panel's Young's modulus, thickness, and Poisson's ratio, respectively. Operators  $(\dot{\cdot})$  and  $(\ddot{\cdot})$ , respectively, represent the first and second derivatives with respect to time.

The equations were solved using the modal decomposition method (Fahy, 1985), incorporating the normalized *in-vacuo* panel eigen-functions  $\varphi_n(x, y)$  for panel mode  $n$ , and *rigid-walled* cavity eigen-functions  $\psi_h(x, y, z)$  for cavity mode  $h$ , and

$$v(x, y, t) = \sum_{n=1}^{\infty} \varphi_n(x, y) \dot{w}_n(t), \quad (3)$$

$$p(x, y, z, t) = -\rho \sum_{h=1}^{\infty} \psi_h(x, y, z) \dot{\phi}_h(t), \quad (4)$$

$$C_{hn} = \int_S \psi_h(x, y, z_0) \varphi_n(x, y) dS, \quad (5)$$

where  $w_n$  is the modal transverse displacement of panel;  $\varphi_h$  is the modal acoustic velocity potential;  $v$  is the panel normal vibration velocity;  $S$  is the area of the panel; and  $C_{hn}$  is the modal fluid-structural coupling coefficient.

The orthogonality properties of eigen-functions are used to decompose the partial differential equations into a set of ordinary differential equations [see Fahy (1985) for details],

$$\alpha_n^2 w_n(t) + 2\zeta_n \alpha_n \dot{w}_n(t) + \ddot{w}_n(t) = \frac{f_n(t)}{m} - \frac{\rho}{m} \sum_{h=1}^{\infty} C_{hn} \dot{\phi}_h(t), \quad (6)$$

$$\begin{aligned} \beta_h^2 \phi_h(t) + 2\zeta_h \beta_h \dot{\phi}_h(t) + \ddot{\phi}_h(t) \\ = c^2 \sum_{n=1}^{\infty} C_{hn} \dot{w}_n(t) - c^2 \psi_h(x_s, y_s, z_s) q(t), \end{aligned} \quad (7)$$

where  $f_n$ ,  $\alpha_n$ , and  $\beta_h$  are the modal force, natural frequencies of *in-vacuo* panel and *rigid-walled* cavity modes, respectively. The proportional damping for the uncoupled panel and cavity modes,  $\zeta_n$  and  $\zeta_h$ , respectively, are incorporated and  $(x_s, y_s, z_s)$  denotes the location of the acoustic volume velocity in the cavity.

## III. OPTIMIZATION OF STRUCTURAL SENSOR PLACEMENT

In practical applications, the panel structure of a coupled panel-cavity system generally has a considerable rigidity for load-carrying purposes and the fluid loading is low, and hence its fluid-structural coupling is generally weak (Pan and Bies, 1990; Cheng, 1994). This situation poses certain challenges in designing virtual sensors for acoustic sensing using structural

sensors. Under such a circumstance, optimal placement of structural sensors can be critical in determining a virtual sensing performance. One of the challenges in this aspect is that the sound pressure dominated by cavity-controlled modes can only be sensed through the fluid-structural coupling by structural sensors. Those modes can be strongly excited under an acoustic excitation. The question is how structural sensors can be strategically placed so as to improve its sensing ability for detecting those modes. To answer it, we proposed an optimization algorithm for sensor placement that is based on modal observability levels of the cavity- and panel-controlled modes.

### A. Sensing cavity-controlled modes

The interior sound pressure response is affected by the spatial nature of acoustic or structural excitation/disturbance. For certain disturbance, some acoustic-structural coupled modes might be strongly excited while others might not. The spatial dependence complicates the task of obtaining a general performance metric since in many cases, the disturbance location is unknown. To deal with such a case, one can consider the use of a spatially varied acoustic source as a disturbance and investigate the structural sensor output to evaluate how “sensitive” the sensor is, at a particular location, in detecting such a disturbance. Such a principle can also be applied for analyzing the effect of spatially varied structural source disturbance to an acoustic sensor inside the cavity thanks to the reciprocity principle.

To do such a task, a sort of performance metric, able to capture the spatially varying characteristic of the disturbance, is required. It is convenient to utilize the spatial  $\mathcal{H}_2$  norm metric that quantifies the spatially averaged output signal energy,  $y$ , of a spatially distributed system under the excitation of a white-noise input (Moheimani *et al.*, 1999),

$$\langle\langle y \rangle\rangle_2^2 = \int_0^\infty \int_\Gamma y(t, r)^T y(t, r) dr d\omega, \quad (8)$$

where  $r \in \Gamma$  is the spatial parameter over the set  $\Gamma$  of all possible spatial locations,  $t$  is the temporal parameter, and  $\omega$  denotes frequency.

In the frequency domain, the weighted spatial  $\mathcal{H}_2$  norm can be calculated from the stable spatially distributed system,  $G(\omega, r)$  (Moheimani *et al.*, 1999),

$$\langle\langle G(\omega, r) \rangle\rangle_2^2 = \frac{1}{2\pi} \int_{-\infty}^\infty \int_\gamma \text{trace} \times \{G(\omega, r)^* Q(r) G(\omega, r)\} dr d\omega, \quad (9)$$

where  $Q(r)$  is the spatial weighting function used to emphasize the spatial region of interest.

#### 1. Structural sensor performance for observing cavity-controlled modes

The ability of the structural sensor to observe cavity-controlled modes is investigated. Let the general structural sensor response,  $y_p$ , be expressed by

$$y_p(t, r_p) = \sum_{n=1}^\infty \{k_{1n}(r_p)w_n(t) + k_{2n}(r_p)\dot{w}_n(t)\}, \quad (10)$$

where  $k_{1n}$  and  $k_{2n}$  are the two structural sensor gains relative to panel modal displacement and velocity and are dependent on the sensor spatial location  $r_p \in \Gamma$ . In this particular case,  $\Gamma$  is the set of all possible sensor locations over the panel area. In its most general form, the structural sensor response is a function of sensor spatially varying location, property, and shape, such as those that may be encountered for piezoelectric-based sensors. From the definition of the  $\mathcal{H}_2$  norm (Zhou *et al.*, 1996), the  $\mathcal{H}_2$  norm of system with multiple structural sensor outputs can be separated into the sum of contributions of individual structural sensor outputs. Thus without losing the generality, the present study focused on the individual sensor placement.

Considering the equation of motion under an acoustic excitation defined by Eq. (7), the second term in the right-hand-side (RHS) dominates so the first RHS term can be ignored, leading to an approximate dynamic model. Let transfer function,  $G_{pq}$ , from spatially varying acoustic point source  $q$  to structural sensor output  $y_p$  be

$$G_{pq}(s, r_p, r_s) = \frac{\rho c^2}{m} \sum_{n=1}^\infty \frac{k_{1n}(r_p) + k_{2n}(r_p)s}{s^2 + 2\zeta_n \alpha_n s + \alpha_n^2} \times \sum_{h=1}^\infty \frac{C_{hm} \psi_h(r_s) s}{s^2 + 2\zeta_h \beta_h s + \beta_h^2}, \quad (11)$$

where  $r_s \triangleq (x_s, y_s, z_s) \in V$  representing the spatial location of an acoustic source over set  $V$  of all possible source locations in the cavity volume. The spatial  $\mathcal{H}_2$  norm of transfer function,  $G_{pq}$ , can be calculated by taking advantage of the orthogonality properties of the acoustic eigen-functions. Here, since we consider the energy under a scalar spatially varying input, the trace operation is not required. In general, the structural output energy due to an acoustic excitation with a certain spatial property can be emphasized using a spatial weighting function  $Q(r_s)$ . By changing the order of summations of  $G_{pq}$  in Eq. (11) the spatial  $\mathcal{H}_2$  norm of  $G_{pq}$  can be written as

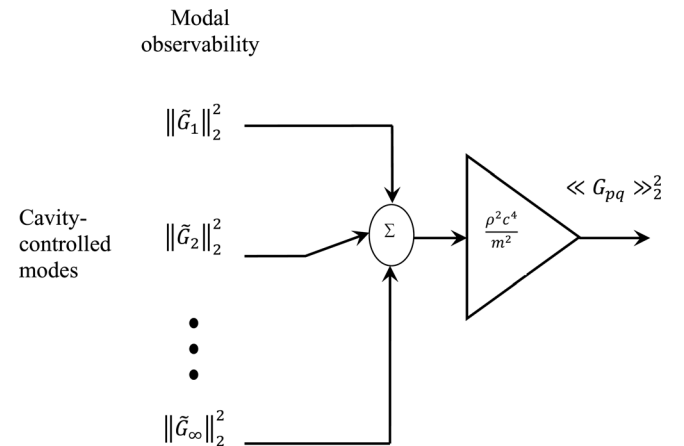


FIG. 2. Contribution of modal observability levels for cavity-controlled modes to the total energy of the spectral-spatial performance metric.

$$\begin{aligned}
\langle\langle G_{pq}(\omega, r_p, r_s) \rangle\rangle_2^2 &= \frac{1}{2\pi} \int_{-\infty}^{\infty} \int_V \{G_{pq}(\omega, r_p, r_s)^* Q(r_s) G_{pq}(\omega, r_p, r_s)\} dr_s d\omega \\
&= \frac{1}{2\pi} \left(\frac{\rho c^2}{m}\right)^2 \int_{-\infty}^{\infty} \int_V \left\{ \left( \sum_{h=1}^{\infty} \frac{-j\omega \psi_h(r_s)}{-\omega^2 - 2\xi_h \beta_h j\omega + \beta_h^2} \sum_{n=1}^{\infty} \frac{C_{hn}(k_{1n}(r_p) - k_{2n}(r_p)j\omega)}{-\omega^2 - 2\xi_n \alpha_n j\omega + \alpha_n^2} \right) \right. \\
&\quad \left. \times \left( \sum_{\bar{h}=1}^{\infty} \frac{j\omega \psi_{\bar{h}}(r_s)}{-\omega^2 + 2\xi_{\bar{h}} \beta_{\bar{h}} j\omega + \beta_{\bar{h}}^2} \sum_{\bar{n}=1}^{\infty} \frac{C_{\bar{h}\bar{n}}(k_{1\bar{n}}(r_p) + k_{2\bar{n}}(r_p)j\omega)}{-\omega^2 + 2\xi_{\bar{n}} \alpha_{\bar{n}} j\omega + \alpha_{\bar{n}}^2} \right) \right\} dr_s d\omega \\
&= \frac{1}{2\pi} \left(\frac{\rho c^2}{m}\right)^2 \int_{-\infty}^{\infty} \sum_{h=1}^{\infty} \left\{ \left( \frac{-j\omega}{-\omega^2 - 2\xi_h \beta_h j\omega + \beta_h^2} \sum_{n=1}^{\infty} \frac{C_{hn}(k_{1n}(r_p) - k_{2n}(r_p)j\omega)}{-\omega^2 - 2\xi_n \alpha_n j\omega + \alpha_n^2} \right) \right. \\
&\quad \left. \times \left( \frac{j\omega}{-\omega^2 + 2\xi_h \beta_h j\omega + \beta_h^2} \sum_{\bar{n}=1}^{\infty} \frac{C_{h\bar{n}}(k_{1\bar{n}}(r_p) + k_{2\bar{n}}(r_p)j\omega)}{-\omega^2 + 2\xi_{\bar{n}} \alpha_{\bar{n}} j\omega + \alpha_{\bar{n}}^2} \right) \right\} d\omega \\
&= \left(\frac{\rho c^2}{m}\right)^2 \sum_{h=1}^{\infty} \|\tilde{G}_h(\omega, r_p)\|_2^2 \tag{12}
\end{aligned}$$

where transfer function  $\tilde{G}_h$  is

$$\begin{aligned}
\tilde{G}_h(s, r_p) &= \left( \frac{s}{s^2 + 2\xi_h \beta_h s + \beta_h^2} \right) \\
&\quad \times \left( \sum_{n=1}^{\infty} \frac{C_{hn}(k_{1n}(r_p) + k_{2n}(r_p)s)}{s^2 + 2\xi_n \alpha_n s + \alpha_n^2} \right). \tag{13}
\end{aligned}$$

Note that if the spatial weighting  $Q(r_s)$  in the first equality is replaced by a Dirac delta function at a specific location, the spatial norm simply reduces to the standard  $\mathcal{H}_2$  norm for an acoustic input located at that location (Moheimani *et al.*, 1999). Although the above norm can be computed numerically, our interest is to look at the general case where the acoustic source is uniformly varied over the entire cavity, thus implying  $Q(r_s) = 1$ .

By taking the spatial  $\mathcal{H}_2$  norm  $\langle\langle G_{qp} \rangle\rangle_2^2$ , we consider the spatially averaged energy transmission from the spatially varying acoustic point source to the structural sensor output. This system norm shows that the overall spatially averaged energy of system is contributed by each cavity-controlled mode as in Eq. (12). For each mode, the energy level is influenced by the contributions of *in-vacuo* panel modes via modal fluid-structural coupling as in Eq. (13). Thus, the contribution of each cavity-controlled mode can be calculated from the standard  $\mathcal{H}_2$  norm of  $\tilde{G}_h$ , i.e.,  $\|\tilde{G}_h\|_2$ . This  $\mathcal{H}_2$  norm can be used as a measure of *modal observability for cavity-controlled modes* that depends on the sensor location as well as other sensor spatial characteristics. Figure 2 depicts the contribution of modal observability levels to the overall energy level due to a spatially varying acoustic source. Thus, the spatial norm can be beneficially used as a performance measure of structural sensing due to cavity-controlled modes because it can be broken down into a number of contributions of those modes.

It should be noted that the additive properties arising from the spatial  $\mathcal{H}_2$  norm in this study differ from those arising from the additive properties of  $\mathcal{H}_2$  or Hankel norms for

purely structural vibration systems, such as the work by Gawronski (1997, 2004) and Smith and Clark (2001). Their work arises from approximating the associated Grammian matrix assuming a lightly damped structure and did not consider the spatial nature of the disturbance input.

Observing transfer function  $\tilde{G}_h$  in Eq. (13), the first multiplicative term acts as a resonant filter that is centered at resonance frequency at which a particular cavity-controlled mode has. The implication of this is that an intuitive method can be used by considering only some panel modes with non-zero modal coupling and resonance frequencies that are close to that of the cavity mode. Another implication of this resonant-like filter is that the contribution of higher frequency modes to  $\langle\langle G_{pq} \rangle\rangle_2^2$  toward the low-frequency band is increasingly less, allowing one to truncate those high frequency modes.

## 2. Target performance of acoustic virtual sensor for observing cavity-controlled modes

Having obtained certain measures to indicate the structural sensor performance, a question may arise on how the structural sensing performance in Eq. (12) can be related to the target acoustic virtual sensing performance. The question is how both sensing performances can be compared so that one knows that a structural sensor has been placed at the best location.

To answer the question, we proposed the following approach to quantify the target virtual sensing performance. To relate the structural sensor results to the target virtual sensing of a sound pressure inside a cavity, one can compare the results with the energy transmission from the spatially varying acoustic source to the acoustic virtual sensor output located at the target virtual sensing location. From the acoustic differential equation in Eq. (7), considering only the dominant acoustic excitation, the transfer function  $G_{vq}$  from spatially varying acoustic point source  $q$  to acoustic sensor output  $y_v$ , at the virtual sensor location  $r_c \triangleq (x_c, y_c, z_c) \in V$ , can be obtained.

Taking the spatial  $\mathcal{H}_2$  norm of  $G_{vq}$  over the cavity volume, one can obtain,

$$\begin{aligned} \langle\langle G_{vq}(\omega, r_c, r_s) \rangle\rangle_2^2 &= \frac{1}{2\pi} \int_{-\infty}^{\infty} \int_V \{G_{vq}(\omega, r_c, r_s)^* \\ &\quad \times G_{vq}(\omega, r_c, r_s)\} dr_s d\omega \\ &= \rho^2 c^4 \sum_h \|\tilde{F}_h(\omega, r_c)\|_2^2, \end{aligned} \quad (14)$$

where

$$\tilde{F}_h(s, r_c) = \frac{s\psi_h(r_c)}{s^2 + 2\zeta_h\beta_h s + \beta_h^2}. \quad (15)$$

In this case, the ability of the acoustic virtual sensor to observe certain cavity-controlled modes can be reflected in terms of  $\|\tilde{F}_h\|_2$ . This norm can be seen as *the target modal observability of the virtual sensor for cavity-controlled modes*. Direct comparison of  $\tilde{F}_h$  with  $\tilde{G}_h$  in Eq. (13) shows that the modal observability of the structural sensor highly depends on the modal coupling and structural sensor arrangement which can complicate the sensor placement, necessitating an optimization process. A similar additive property of  $\langle\langle G_{vq} \rangle\rangle_2^2$  can be depicted as in Fig. 2 by, respectively, substituting  $\tilde{G}_h$  and  $(\frac{\rho c^2}{m})^2$  with  $\tilde{F}_h$  and  $\rho^2 c^4$ .

## B. Sensing panel-controlled modes

### 1. Structural sensor performance for observing panel-controlled modes

A similar method was used for analyzing the ability of a structural sensor at a particular location in detecting panel-controlled modes. When the spatial  $\mathcal{H}_2$  norm is calculated with respect to spatially varying point structural force, the modal force term dominates over the coupling term in the RHS of Eq. (6). Therefore an approximation to the differential equation can be used to obtain the relevant transfer function from the structural force to the sensor output  $y_p$ .

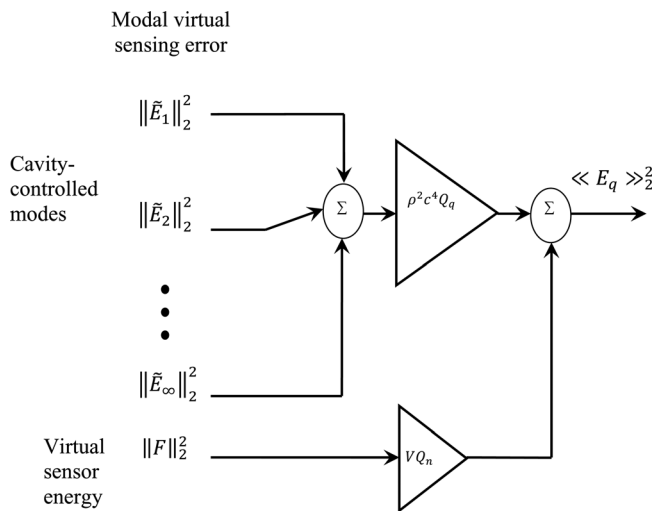


FIG. 3. Contribution of modal virtual sensing error for cavity-controlled modes and the virtual sensor filter energy to the total energy of the spectral-spatial virtual sensing error performance metric.

Taking the spatial  $\mathcal{H}_2$  norm with respect to spatially varying point structural force over the panel area,  $r_f \triangleq (x_f, y_f) \in S$ ,

$$\begin{aligned} \langle\langle G_{pf}(\omega, r_p, r_f) \rangle\rangle_2^2 &= \frac{1}{2\pi} \int_{-\infty}^{\infty} \int_S \{G_{pf}(\omega, r_p, r_f)^* \\ &\quad \times G_{pf}(\omega, r_p, r_f)\} dr_f d\omega \\ &= \frac{1}{m^2} \sum_{n=1}^{\infty} \|\bar{G}_n(\omega, r_p, r_f)\|_2^2, \end{aligned} \quad (16)$$

where  $G_{pf}$  is the transfer function from  $f$  to  $y_p$  with

$$\bar{G}_n(s, r_p) = \frac{k_{1n}(r_p) + k_{2n}(r_p)s}{s^2 + 2\zeta_n\alpha_n s + \alpha_n^2}. \quad (17)$$

The  $\mathcal{H}_2$  norm of  $\bar{G}_n$  can thus be regarded as a measure of *modal observability for panel-controlled modes*. Here, the result is straightforward since it only considers the direct effect of structural force to the structural sensor outputs where the panel-controlled modes are dominant. Such additive properties of the spatial  $\mathcal{H}_2$  norm have been observed by Halim and Moheimani (2003), although their study considered the case for structural vibration systems only. In the present work, vibro-acoustic systems are focused on and contributions of both the panel- and cavity-controlled modes are considered as a whole, together with their target modal observability levels for the virtual sensor. The additive property of  $\langle\langle G_{pf} \rangle\rangle_2^2$  can be shown as in Fig. 2 using substitutions of  $\bar{G}_n$  and  $\frac{1}{m^2}$  for  $\tilde{G}_h$  and  $(\frac{\rho c^2}{m})^2$ .

### 2. Target performance of acoustic virtual sensor for observing panel-controlled modes

Considering the energy transmission from spatially varying force to the acoustic virtual sensor outputs, one can also obtain similar results by considering the modal forcing term that dominates over the acoustic coupling term. From Eqs. (6) and (7), the transfer function from  $f$  to  $y_v$ ,  $G_{vf}$  can be determined and the spatial  $\mathcal{H}_2$  norm can be calculated by changing the order of summations and taking advantage the orthogonality condition of structural eigen-functions over the area of panel,

TABLE I. First 20 natural frequencies of a coupled panel-cavity system [ $n$  or  $h$  indicate the  $n$ th panel-controlled or  $h$ th cavity-controlled modes (shown in bold), respectively].

$n$ (panel)	Freq. (Hz)	$n$ (panel)	Freq. (Hz)	$h$ (cavity)	Freq. (Hz)
1 (1, 1)	31.6	7 (1, 4)	181.6	<b>1 (0,0)</b>	<b>0.0</b>
2 (1, 2)	59.8	8 (3, 1)	188.8	<b>2 (0,1)</b>	<b>145.9</b>
3 (2, 1)	89.2	9 (3, 2)	218.4	<b>3 (0,1,0)</b>	<b>175.9</b>
4 (1, 3)	110.3	10 (2, 4)	240.3	<b>4 (0,1,1)</b>	<b>229.7</b>
5 (2, 2)	119.6	11 (3, 3)	269.1	<b>5 (1,0,0)</b>	<b>248.1</b>
6 (2, 3)	169.9	12 (1, 5)	271.3	<b>6 (1,0,1)</b>	<b>287.4</b>
				<b>7 (0,0,2)</b>	<b>290.7</b>
				<b>8 (1,1,0)</b>	<b>304.5</b>

$$\begin{aligned}
\langle\langle G_{vf}(\omega, r_c, r_f) \rangle\rangle_2^2 &= \frac{1}{2\pi} \int_{-\infty}^{\infty} \int_S \{G_{vf}(\omega, r_c, r_f)^* G_{vf}(\omega, r_c, r_f)\} dr_f d\omega \\
&= \frac{1}{2\pi} \left(\frac{\rho c^2}{m}\right)^2 \int_{-\infty}^{\infty} \int_S \left\{ \begin{aligned} &\left( \sum_{h=1}^{\infty} \frac{-\omega^2 \psi_h(r_c)}{-\omega^2 - 2\xi_h \beta_h j\omega + \beta_h^2} \sum_{n=1}^{\infty} \frac{C_{hn} \phi_n(r_f)}{-\omega^2 - 2\xi_n \alpha_n j\omega + \alpha_n^2} \right) \\ &\times \left( \sum_{h=1}^{\infty} \frac{\omega^2 \psi_h(r_c)}{-\omega^2 + 2\xi_h \beta_h j\omega + \beta_h^2} \sum_{n=1}^{\infty} \frac{C_{hn} \phi_n(r_f)}{-\omega^2 + 2\xi_n \alpha_n j\omega + \alpha_n^2} \right) \end{aligned} \right\} dr_f d\omega \\
&= \frac{1}{2\pi} \left(\frac{\rho c^2}{m}\right)^2 \int_{-\infty}^{\infty} \int_S \left\{ \begin{aligned} &\left( \sum_{n=1}^{\infty} \frac{-\omega^2 \phi_n(r_f)}{-\omega^2 - 2\xi_n \alpha_n j\omega + \alpha_n^2} \sum_{h=1}^{\infty} \frac{C_{hn} \psi_h(r_c)}{-\omega^2 - 2\xi_h \beta_h j\omega + \beta_h^2} \right) \\ &\times \left( \sum_{n=1}^{\infty} \frac{\omega^2 \phi_n(r_f)}{-\omega^2 + 2\xi_n \alpha_n j\omega + \alpha_n^2} \sum_{h=1}^{\infty} \frac{C_{hn} \psi_h(r_c)}{-\omega^2 + 2\xi_h \beta_h j\omega + \beta_h^2} \right) \end{aligned} \right\} dr_f d\omega \\
&= \left(\frac{\rho c^2}{m}\right)^2 \sum_{n=1}^{\infty} \|\bar{F}_n(\omega, r_c)\|_2^2, \tag{18}
\end{aligned}$$

with

$$\begin{aligned}
\bar{F}_n(s, r_c) &= \left( \frac{1}{s^2 + 2\xi_n \alpha_n s + \alpha_n^2} \right) \\
&\times \left( \sum_{h=1}^{\infty} \frac{C_{hn} \psi_h(r_c) s^2}{s^2 + 2\xi_h \beta_h s + \beta_h^2} \right). \tag{19}
\end{aligned}$$

The first multiplicative term in Eq. (19) is a resonant filter, indicating that the impact of *rigid-walled* cavity modes is influenced by both their modal-coupling and how close their resonance frequencies to that of the *in-vacuo* panel modes. Using a similar reasoning as in the case of cavity-controlled modes,  $\|\bar{F}_n(\omega, r_c)\|_2$  can be used as a measure of *panel-controlled modal observability*, describing how much energy transmitted from the structural force input to the structural sensor output. The additive property of  $\langle\langle G_{vf} \rangle\rangle_2^2$  has a similar form as that for the cavity-controlled modes in Fig. 2.

### C. Influence of modal observability metric on the virtual sensing performance

Here, we consider a general case of virtual sensor filter  $F(\omega)$  that is stable, causal, and linear time-invariant. The effect of noise in the structural sensor measurements is also considered to evaluate how the measurement noise can impact the sensing performances. Again, we initially investigated the virtual sensing performances for the cavity- and panel-controlled modes, respectively. Later, an optimization problem is set-up based on the consideration of both types of modes.

#### 1. Modal virtual sensing error for cavity-controlled modes

We consider the virtual sensing error due to a white-noise spatially varying acoustic input, whose sensing error transfer function can be shown after changing the summation order of  $G_{pq}$ ,

$$\begin{aligned}
G_{vq}(s, r_s, r_c) - F(s)G_{pq}(s, r_p, r_s) \\
&= \rho c^2 \sum_{n=1}^{\infty} \frac{\psi_h(r_s) s}{s^2 + 2\xi_n \beta_h s + \beta_h^2} \\
&\times \left\{ \psi_h(r_c) - \frac{F(s)}{m} \sum_{n=1}^{\infty} \frac{c_{hn}(k_{1n}(r_p) + k_{2n}(r_p)s)}{s^2 + 2\xi_n \alpha_n s + \alpha_n^2} \right\}. \tag{20}
\end{aligned}$$

By calculating its spatial  $\mathcal{H}_2$  norm over the cavity volume, it yields

$$\begin{aligned}
\langle\langle G_{vq}(\omega, r_s, r_c) - F(\omega)G_{pq}(\omega, r_p, r_s) \rangle\rangle_2^2 \\
&= \rho^2 c^4 \sum_{h=1}^{\infty} \|\tilde{E}_h(\omega, r_p, r_c)\|_2^2, \tag{21}
\end{aligned}$$

where transfer function  $\tilde{E}_h$  can be defined as *the modal virtual sensing error system* for the  $h$ th cavity-controlled mode,

$$\begin{aligned}
\tilde{E}_h(s, r_p, r_c) &= \frac{s}{s^2 + 2\xi_h \beta_h s + \beta_h^2} \left\{ \psi_h(r_c) \right. \\
&\quad \left. - \frac{F(s)}{m} \sum_{n=1}^{\infty} \frac{C_{hn}(k_{1n}(r_p) + k_{2n}(r_p)s)}{s^2 + 2\xi_n \alpha_n s + \alpha_n^2} \right\} \\
&= \tilde{F}_h(s, r_c) - \frac{F(s)}{m} \tilde{G}_h(s, r_p). \tag{22}
\end{aligned}$$

The second term in the above equation is calculated by considering that the virtual sensor filter is independent of acoustic input locations. Both terms  $\tilde{F}_h$  and  $\tilde{G}_h$  have been defined previously in Eqs. (15) and (13), respectively.

Next, consider the case where the spatially varying acoustic and measurement inputs are white, zero-mean, Gaussian, and uncorrelated, with the diagonal spectral density matrices  $Q_q$  and  $Q_n$ , respectively. The error sensing system due to the acoustic disturbance (process noise) and measurement noise inputs, was defined as  $E_q$ . Taking the spatial  $\mathcal{H}_2$  norm of the system over the entire cavity volume, incorporating Eq. (21), we obtain,

$$\begin{aligned}
\langle\langle E_q(\omega, r_p, r_c) \rangle\rangle_2^2 &= \frac{1}{2\pi} \int_{-\infty}^{\infty} \int_V \text{trace}\{E_q(\omega, r_p, r_s, r_c)^* E_q(\omega, r_p, r_s, r_c)\} dr_s d\omega \\
&= \langle\langle [G_{vq}(\omega, r_s, r_c) \sqrt{Q_q} \mathbf{0}] - F(\omega) [G_{pq}(\omega, r_p, r_s) \sqrt{Q_q} \sqrt{Q_n}] \rangle\rangle_2^2 \\
&= \frac{1}{2\pi} \int_{-\infty}^{\infty} \int_V \left\{ Q_q (G_{vq}(\omega, r_s, r_c) - F(\omega) G_{pq}(\omega, r_p, r_s))^* \right. \\
&\quad \left. \times (G_{vq}(\omega, r_s, r_c) - F(\omega) G_{pq}(\omega, r_p, r_s)) + Q_n F(\omega)^* F(\omega) \right\} dr_s d\omega \\
&= Q_q \langle\langle G_{vq}(\omega, r_s, r_c) - F(\omega) G_{pq}(\omega, r_p, r_s) \rangle\rangle_2^2 + Q_n V \|F(\omega)\|_2^2 \\
&= \rho^2 c^4 Q_q \sum_{h=1}^{\infty} \left\| \tilde{F}_h(\omega, r_c) - \frac{F(\omega)}{m} \tilde{G}_h(\omega, r_p) \right\|_2^2 + Q_n V \|F(\omega)\|_2^2 \\
&= \rho^2 c^4 Q_q \sum_{h=1}^{\infty} \|\tilde{E}_h(\omega, r_p, r_c)\|_2^2 + Q_n V \|F(\omega)\|_2^2. \tag{23}
\end{aligned}$$

The above equation indicates that for the cavity-controlled mode case, the energy of virtual sensing error system can be expressed as a simple summation of contribution of each modal sensing error  $\|\tilde{E}_h(\omega, r_p, r_c)\|_2^2$  and the measurement noise. Although the virtual sensor filter  $F(\omega)$  is not yet defined, it can be seen that the structural sensor placement strategy is highly influenced by the modal observability levels characterized by  $\tilde{F}_h$  and  $\tilde{G}_h$ . Figure 3 depicts the contributions of each modal virtual sensor error energy to the overall virtual sensing

error energy for cavity-controlled modes. It showed the effect of the virtual sensor filter energy in contributing to the virtual sensing accuracy.

## 2. Modal virtual sensing error for panel-controlled modes

Similarly, for the case of panel-controlled modes, the virtual sensing due to spatially varying structural input is considered after changing the summation order of  $G_{pf}$ ,

$$G_{vf}(s, r_c, r_f) - F(s) G_{pf}(s, r_p, r_c, r_f) = \frac{1}{m} \sum_{n=1}^{\infty} \frac{\varphi_n(r_f)}{s^2 + 2\zeta_n \alpha_n s + \alpha_n^2} \left\{ -\rho c^2 \sum_{h=1}^{\infty} \frac{c_{hn} \psi_h(r_c) s^2}{s^2 + 2\zeta_h \beta_h s + \beta_h^2} - F(s) (k_{1n}(r_p) + k_{2n}(r_p) s) \right\}. \tag{24}$$

Consider the case where the white-noise spatially varying structural input and measurement noise whose strength levels are described by diagonal spectral density matrices  $Q_f$  and  $Q_n$ , respectively. Taking the spatial  $\mathcal{H}_2$  norm of error sensing  $E_f$  due to the spatially varying input and measurement noise, one can derive,

$$\begin{aligned}
\langle\langle E_f(\omega, r_p, r_c) \rangle\rangle_2^2 &= \frac{1}{2\pi} \int_{-\infty}^{\infty} \int_S \text{trace}\{E_f(\omega, r_p, r_c, r_f)^* E_f(\omega, r_p, r_c, r_f)\} dr_f d\omega \\
&= \langle\langle [G_{vf}(\omega, r_c, r_f) \sqrt{Q_f} \mathbf{0}] - F(\omega) [G_{pf}(\omega, r_p, r_f) \sqrt{Q_f} \sqrt{Q_n}] \rangle\rangle_2^2 \\
&= Q_f \langle\langle G_{vf}(\omega, r_f) - F(\omega) G_{pf}(\omega, r_p, r_f) \rangle\rangle_2^2 + Q_n S \|F(\omega)\|_2^2 = \frac{Q_f}{m^2} \sum_{n=1}^{\infty} \|\bar{E}_n(\omega, r_p, r_c)\|_2^2 + Q_n S \|F(\omega)\|_2^2, \tag{25}
\end{aligned}$$

where transfer function  $\bar{E}_n$  is the modal virtual sensing error system for the  $n$ th panel-controlled mode,

$$\begin{aligned}
\bar{E}_n(s, r_p, r_c) &= \frac{1}{s^2 + 2\zeta_n \alpha_n s + \alpha_n^2} \left\{ -\rho c^2 \sum_{h=1}^{\infty} \frac{C_{hn} \psi_h(r_c) s^2}{s^2 + 2\zeta_h \beta_h s + \beta_h^2} \right. \\
&\quad \left. - F(s) (k_{1n}(r_p) + k_{2n}(r_p) s) \right\} \\
&= -\rho c^2 \bar{F}_n(s, r_c) - F(s) \bar{G}_n(s, r_p) \tag{26}
\end{aligned}$$

and both terms  $\bar{F}_n$  and  $\bar{G}_n$  are defined by Eqs. (19) and (17), respectively. Similar to the cavity-controlled mode case, the error sensing of the virtual sensors can be expressed as a simple summation of contribution of each modal error sensing  $\|\bar{E}_n(\omega, r_p, r_c)\|_2^2$  and the measurement noise. The contributions of the modal virtual sensing error energy for the panel-controlled modes can be depicted as in Fig. 3, by, respectively, substituting  $\rho^2 c^4 Q_q$ ,  $\tilde{E}_h$ , and  $V Q_n$  with  $\frac{Q_f}{m^2}$ ,  $\bar{E}_n$ , and  $S Q_n$ .

### 3. Aspects of virtual sensor performance

The virtual sensing error results in Eqs. (23) and (25) showed that the spatially averaged energy of virtual sensing error system is mainly influenced by (a) the modal sensing error, (b) the ratio of process noise to measurement noise, and (c) the virtual sensor filter.

*a. The modal virtual sensing error.* The first terms of the virtual sensing errors in Eqs. (23) and (25) describe the contributions of modal virtual sensing errors to the overall virtual sensing error, for either panel- or cavity-controlled modes. The modal virtual sensing error highly depends on the structural sensor spatial placement and properties. This modal error description can help simplify the structural sensor placement process because what one needs to do is to find a sensor location with certain modal observability properties, which would help in reducing the dominant modal virtual sensing error levels.

Also note that each of  $\bar{G}_n$ ,  $\tilde{G}_h$ ,  $\bar{F}_n$ , and  $\tilde{F}_h$  system consists of a dominant resonant-like filter centered at the corresponding resonance frequency. Thus the  $\mathcal{H}_2$  norm used for its modal observability metric also reflects the maximum gain related to their sensing sensitivity. If a panel- or cavity-controlled mode does not have sufficiently high observability levels (described by  $\|\bar{G}_n\|_2$  and  $\|\tilde{G}_h\|_2$ ) while the target virtual sensing modal observability levels are high (described by  $\|\bar{F}_n\|_2$  and  $\|\tilde{F}_h\|_2$ ), then the required virtual sensor filter gain  $F(\omega)$  to minimize the modal virtual sensing error would be large. The results also show the fundamental limitation of the virtual sensor error. From the modal virtual sensing error systems in Eqs. (22) and (26), ideally the structural and acoustic modal observability functions should have similar spectral shapes, particularly near and at the resonance of the mode of interest. In this case, a constant virtual sensor gain can be simply used to force the modal virtual sensing error to very close to zero. However, the two modal observability functions have different spectral shapes, in which one of them is filtered by a contribution of coupled modes. This complicates the task of achieving small sensing error and necessitates a frequency dependent virtual sensor gain.

*b. The ratio of process noise strength to measurement noise strength.* The second terms in the virtual sensing error expressions describe the impact of sensor measurement noise to the structural sensing. The higher the measurement noise strength  $Q_n$  relative to the process noise strength,  $Q_q$  and  $Q_f$ , the higher is the level of virtual sensing error.

*c. The virtual sensor filter.* The modal virtual sensing error systems  $\tilde{E}_h$  and  $\tilde{E}_n$  in Eqs. (22) and (26) are described for a generic virtual sensor filter  $F(\omega)$ . It can be seen from the results that the virtual sensing error is amplified by the overall virtual sensor filter gain  $F(\omega)$ . Thus, a relatively low sensor filter gain would be desirable and a relatively high signal-to-noise ratio for structural sensors used can improve the virtual sensing accuracy. These results also illustrate the importance of modal observability metrics for developing an optimization method for structural sensor placement so that sufficiently high modal observability levels can be achieved for certain important modes.

Furthermore, in the case where the panel vibration is small such as at its anti-resonance frequencies, the virtual sensor filter gain needs to be large to achieve a small virtual sensing error at those frequencies. If the filter gain is not high enough, the virtual sensing accuracy degrades, leading to a poor active control performance. However, the structural sensor noise will be amplified as a consequence of high filter gain. This situation emphasizes the importance of the proposed optimization methodology to avoid small observability levels for important panel- or cavity-controlled modes. This way, small panel vibration can be avoided at or near resonance frequencies associated with those modes. Thus, the virtual sensor filter gain can be moderated to reduce the sensor noise sensitivity and the modes of interest can be observed and controlled effectively.

### D. Optimization method for structural sensor placement

Based on the above results, it is possible to find a structural sensor placement that satisfies certain sensing requirements. Some of the low-frequency cavity-controlled modes are important for active control of a coupled panel-cavity system, when the main disturbance source is of acoustic nature. On the other hand, when the main disturbance is structural, both panel and cavity-controlled modes can dominate particularly at frequencies near the resonances. Hence, both types of modes need to be considered in the optimization process. In the virtual sensor implementation, we can only include some of the important low-frequency modes, because the contributions of higher frequency modes are less dominant than those of low frequency as previously discussed. Hence, it is reasonable in practice to truncate those higher frequency modes. A compromise is required because for each particular location of sensor, modal observability levels of each mode vary, indicating that it may not be possible to achieve reasonably high levels at the same time.

Selecting certain low-frequency panel- and cavity-controlled modes, the spatial norms can be approximated by truncating the infinite terms in Eqs. (12), (14), (16), and (18). In terms of the contribution of each mode to the overall target virtual sensing output energy, one can use the *normalized squared modal observability* from Eqs. (14) and (18),

$$\tilde{k}_h(r_c) \triangleq \frac{\|\tilde{F}_h(\omega, r_c)\|_2^2}{\sum_{h=2}^{h_m} \|\tilde{F}_h(\omega, r_c)\|_2^2} \quad \forall h = 2, \dots, h_m, \quad (27)$$

$$\bar{k}_n(r_c) \triangleq \frac{\|\bar{F}_n(\omega, r_c)\|_2^2}{\sum_{n=1}^{n_m} \|\bar{F}_n(\omega, r_c)\|_2^2} \quad \forall n = 1, \dots, n_m, \quad (28)$$

where  $h_m$  and  $n_m$  are respectively the highest mode numbers of interest for the cavity- and panel-controlled modes. Further,  $\tilde{k}_h(r_c)$  and  $\bar{k}_n(r_c)$  are the modal observability levels of the cavity- and panel-controlled modes for the target acoustic virtual sensing, respectively, both of which depend on the virtual sensor location  $r_c$ .

In terms of  $\tilde{k}_h$  and  $\bar{k}_n$ , one can evaluate the level of importance for cavity- or panel-controlled modes. Because it may not be possible to optimize all modal observability levels, it is important to select certain important modes. Normalizing all the parameters with respect to their maximum values over the possible locations for a structural sensor,

$$\Omega_q(r_p) \triangleq \frac{\langle\langle G_{pq}(\omega, r_p) \rangle\rangle_2}{\max_{r_p \in \Gamma} \langle\langle G_{pq}(\omega, r_p) \rangle\rangle_2}, \quad (29)$$

$$\tilde{g}_h(r_p) \triangleq \frac{\|\tilde{G}_h(\omega, r_p)\|_2}{\max_{r_p \in \Gamma} \|\tilde{G}_h(\omega, r_p)\|_2}, \quad (30)$$

$$\Pi_f(r_p) \triangleq \frac{\langle\langle G_{pf}(\omega, r_p) \rangle\rangle_2}{\max_{r_p \in \Gamma} \langle\langle G_{pf}(\omega, r_p) \rangle\rangle_2}, \quad (31)$$

$$\bar{g}_n(r_p) \triangleq \frac{\|\bar{G}_n(\omega, r_p)\|_2}{\max_{r_p \in \Gamma} \|\bar{G}_n(\omega, r_p)\|_2}, \quad (32)$$

where  $\Omega_q(r_p)$ ,  $\Pi_f(r_p)$ ,  $\tilde{g}_h(r_p)$ , and  $\bar{g}_n(r_p)$  can be defined as the spatially averaged observability of the cavity- and panel-controlled modes, and the modal observability levels of the cavity- and panel-controlled modes, respectively. Those parameters depend on the structural sensor location  $r_p$  that needs to be optimized over the area of a flexible panel in the coupled enclosure.

An optimization was set-up to determine the optimal location for structural sensors by considering the observability levels contributed by the cavity- and panel-controlled modes. Selection of parameters can be done by comparing the relative strength of modal observability levels for the target acoustic virtual sensing. A scalar weighting term  $v$  is introduced to weigh the contribution of cavity-controlled modes relative to the panel-controlled modes. The optimization problem for finding the optimal structural sensor location is described as

$$\max_{r_p \in \Gamma} v \Omega_q(r_p) + (1 - v) \Pi_f(r_p), \quad (33)$$

subject to the following cavity- and panel-controlled modal observability constraints,

$$\tilde{g}_h(r_p) \geq \tilde{\sigma}_h \vee h = 2, \dots, h_m, \quad (34)$$

$$\bar{g}_n(r_p) \geq \bar{\sigma}_n \vee n = 1, \dots, n_m, \quad (35)$$

where  $\tilde{\sigma}_h$  and  $\bar{\sigma}_n$  represent the upper limits for the modal observability for the cavity- and panel-controlled modes, respectively.

The constraints are used to ensure that the modal observability levels of important modes are sufficiently high. Alternatively, other modes which are not sensing priorities, such as the off-bandwidth modes, can be suppressed by adjusting modal constraints in a similar way, to avoid the effect of sensing spillover that can degrade control performance. The optimization problem can thus be solved to find the structural sensor locations that satisfy the above constraints. Since multiple minima may occur, a number of ini-

tial sensor locations can be used to obtain the global minimum.

The proposed virtual sensor system can be used for both active control of internal noise source and sound transmission. In the case of active control of sound transmission, the acoustic response in the acoustic-structural coupled cavity is mainly dominated by the panel-controlled modes. Acoustic modes also amplify the acoustic field at acoustic resonances. For structural modes, structural sensors can be effective in detecting these modes that are dominated by the panel vibration. It is sufficient to place the sensors at the locations that can effectively observe relevant panel modes, such as placing at or near the anti-nodes of panel mode shapes. This can be done by optimizing some measures of modal observability for panel-controlled modes in Eqs. (16) and (17), which are formalized in  $\Pi_f$  and  $\bar{g}_n$  in Eqs. (31)–(32). This may require an optimization if several panel-controlled modes are of interest. Acoustic modes are sensed through the feedback reaction of the acoustic pressure on the panel vibration. In the case of internal noise source, the acoustic response in the cavity is dominated by the cavity-controlled modes. Since these modes are indirectly sensed via acoustic-structural coupling, the optimization for the structural sensor placement is more complicated than that for the active control of sound transmission case. The optimization methodology presented in this work, as summarized in Eqs. (33)–(35), thus becomes important.

#### IV. NUMERICAL STUDY ON STRUCTURAL SENSOR PLACEMENT

The performance analysis was conducted on a rectangular coupled panel-cavity system with dimensions of 0.695 m  $\times$  0.976 m  $\times$  1.188 m with one side at  $z_0 = 0$ , on the  $x$ - $y$  plane, covered by a simply supported aluminum panel of size (0.695 m  $\times$  0.976 m) and thickness of 4 mm. Modal proportional damping ratios used are 0.005 and 0.003 for structural and cavity modes, respectively. The acoustic virtual sensor inside the cavity was located at  $(x_c, y_c, z_c) = (0.070$  m, 0.816 m, 1.028 m) as shown in Fig. 1. A structural velocity sensor was used in this numerical analysis. Table I shows the natural frequencies of the first 20 coupled panel-cavity modes.

##### A. Structural sensor placements

Figure 4 shows the normalized squared modal observability levels,  $\tilde{k}_h$  and  $\bar{k}_n$ , that describe the relative contribution to the spatial norm. The first 12 panel-controlled, and the second to eighth cavity-controlled modes have been incorporated in the calculation. For this acoustic virtual sensing location, only the first, seventh, and ninth panel-controlled modes dominate the sensing energy, while the second to eighth cavity-controlled modes, with the exception of the seventh mode, have comparable contributions.

Figures 5(a)–5(e) show the normalized modal observability for the cavity-controlled modes as a function of the structural sensor location, for the second to sixth modes, respectively. The effect of modal coupling is apparent on the observability plots. For the second cavity-controlled mode

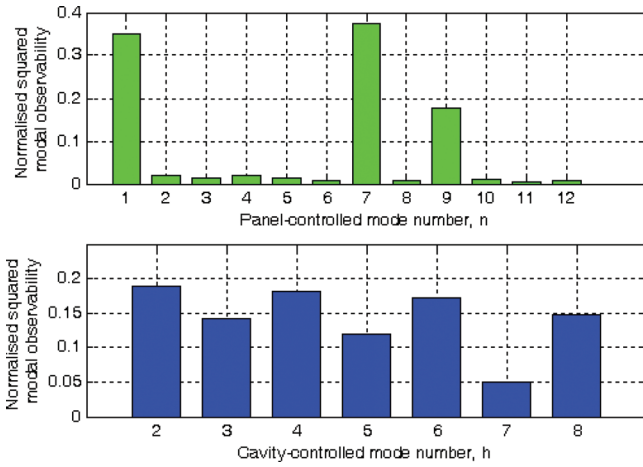


FIG. 4. (Color online) Normalized squared modal observability levels for panel-controlled modes,  $\tilde{k}_n$  with  $n = 1, \dots, 12$ , and cavity-controlled modes,  $\tilde{k}_h$  with  $h = 2, \dots, 8$ , for the target acoustic sensing at the virtual sensor location (0.070 m, 0.816 m, 1.028 m).

dominated by cavity mode (0,0,1) [Fig. 5(a)], the first few structural modes of modes (1,1), (1,3), and (3,1) contribute dominantly to the modal observability level because those modes have non-zero fluid-structural coupling. Apart of the modal coupling, the resonance frequency of the *in-vacuo* structural mode relative to that of the *rigid-walled* cavity

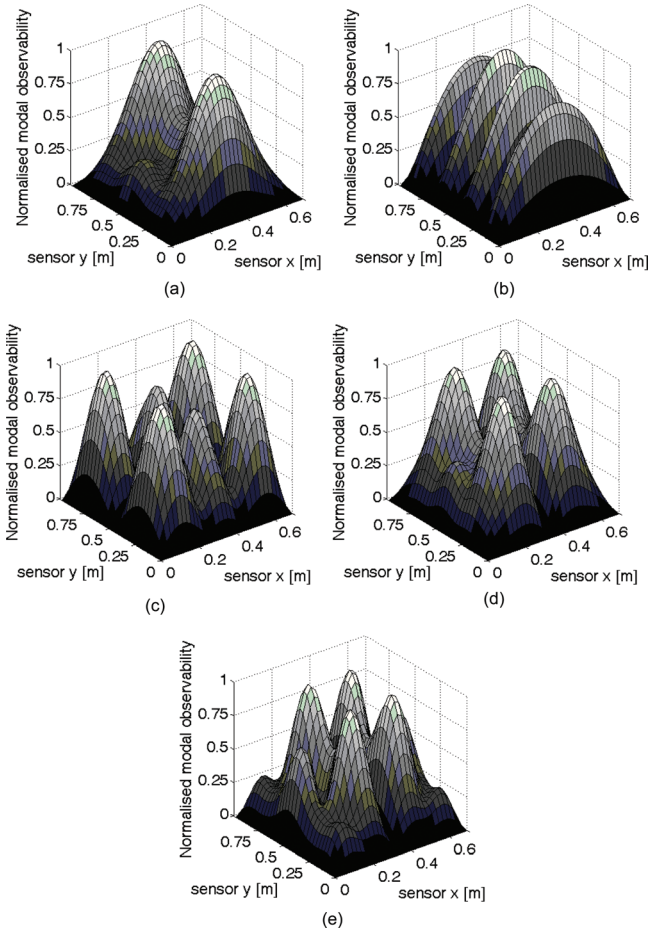


FIG. 5. (Color online) Normalized modal observability for cavity-controlled modes,  $\tilde{g}_h$ , for various structural sensor locations: (a)  $\tilde{g}_2$  for the second mode, (b)  $\tilde{g}_3$  for the third mode, (c)  $\tilde{g}_4$  for the fourth mode, (d)  $\tilde{g}_5$  for the fifth mode, and (e)  $\tilde{g}_6$  for the sixth mode.

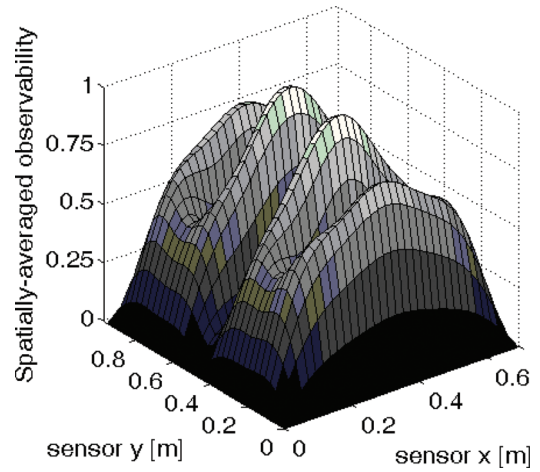
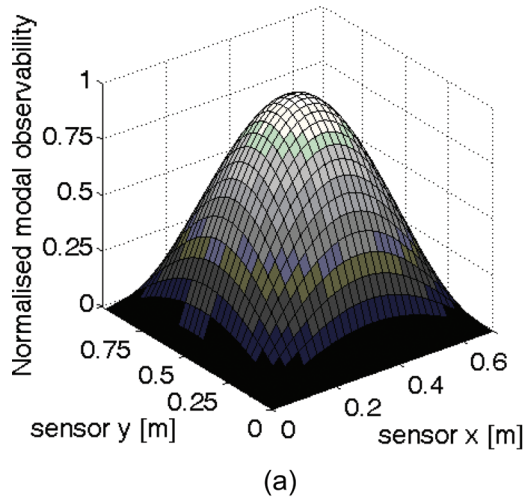


FIG. 6. (Color online) Normalized spatial observability for cavity-controlled modes,  $\Omega_q$ , for various structural sensor locations, contributed by the second to sixth cavity-controlled modes.

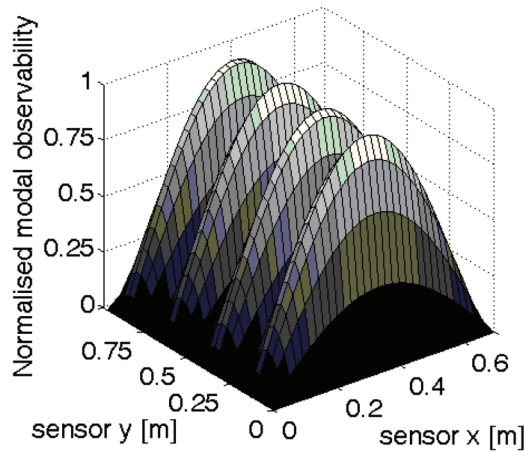
mode also impacts on the observability level. Here, the structural mode (1,3) is dominant because its resonance frequency is the closest to the cavity mode (0,0,1). More dominant effects are the panel modes (1,4), (3,2), and (2,3) to the third, fourth, and fifth cavity-controlled modes, respectively. The spatial observability contributed by those modes is plotted as a function of sensor location in Fig. 6, showing the variation of the normalized spatially averaged observability as a function of structural sensor location. Obvious variations, sometimes even drastic, show the strong dependence of the cavity-controlled modal sensing to the structural sensor location.

For the first, seventh, and ninth panel-controlled modes, the normalized modal observability plots are shown in Figs. 7(a)–7(c), respectively. The modal observability profiles are straightforward, related directly to the *in-vacuo* structural eigen-functions. When considering structural vibration alone, a discrete structural sensor can be placed at the anti-nodes of structural eigen-functions. However, for vibro-acoustic applications proposed in this work, both the cavity- and panel-controlled modes should be taken into account. Figure 8 depicts the normalized spatial observability of those panel-controlled modes. In contrast to the spatial observability for the cavity-controlled modes shown in Fig. 6, less variation was observed for the panel-controlled modes because of the dominance of the first panel mode.

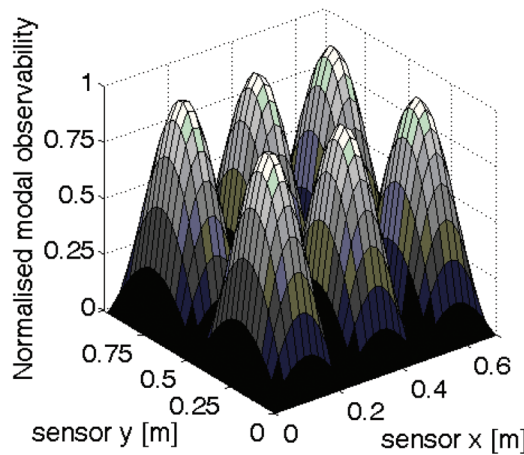
The constrained optimization problem in Eqs. (33)–(35) was set-up. A scalar weighting term  $\nu = 0.5$  was used, so equal contributions of cavity- and panel-controlled modes were considered. The upper limits for constraints in Eqs. (34) and (35) were set to 0.5, meaning that the normalized observability of each mode was at least 50% to ensure reasonable detection of those modes of interest. The optimization result was sensitive to these constraints. If the upper limits were set too low, some modes might have low observability levels. On the other, if the limits were set too high, there might be no feasible optimization solution due to excessive constraints. A number of initial locations of structural sensor were used in the optimization, since in general



(a)



(b)



(c)

FIG. 7. (Color online) Modal observability for panel-controlled modes,  $\bar{g}_n$ , for various structural sensor locations: (a)  $\bar{g}_1$  for the first mode, (b)  $\bar{g}_7$  for the seventh mode, and (c)  $\bar{g}_9$  for the ninth mode.

the performance function was not convex. Figure 9 shows modal observability levels, normalized to their maximum observability levels, for the optimal sensor location at (0.297 m, 0.360 m). The results show that those modes of priority have relatively high levels, considering that the maximum level achievable is 1. The structural sensor location in the

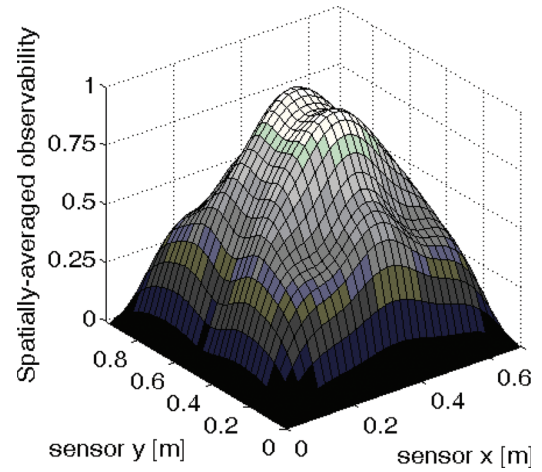


FIG. 8. (Color online) Normalized spatial observability of panel-controlled modes,  $\Pi_r$ , for various structural sensor locations, contributed by the first, seventh, and ninth panel-controlled modes.

panel-cavity system, relative to the acoustic virtual sensor location, is depicted in Fig. 1.

The magnitude frequency responses from an acoustic volume-velocity source at (0.430 m, 0.330 m, 0.850 m) to the acoustic virtual sensor and structural sensor outputs are shown in Fig. 10(a) and Figs. 10(b)–10(c), respectively. At the acoustic virtual sensor location inside the cavity, the second to sixth cavity-controlled modes (indicated by  $\odot$ ) are clearly observable, which means that it was desirable for the structural sensing to be sensitive in detecting those modes. Figures 10(b) and 10(c) show that the structural sensor at the optimized location had relatively high responses at the resonances of modes of interest, particularly for the second to sixth cavity-controlled modes. A low response at resonance for the seventh mode (290.7 Hz) was observed since the seventh mode was not included in the optimization process. Figures 10(b) and 10(c) compare the structural sensing performance for the sensor at the optimized location with structural sensors at different locations: location 1 (0.173 m, 0.196 m), location 2 (0.640 m, 0.300 m), location 3 (0.510 m,

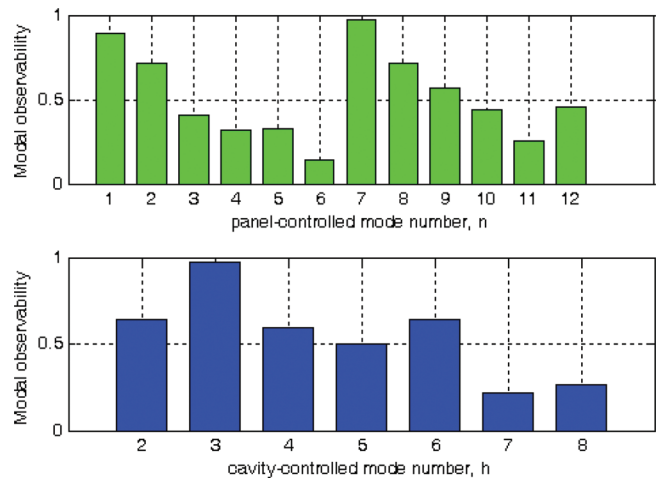


FIG. 9. (Color online) Normalized modal observability levels for panel-controlled modes,  $\bar{g}_n$ , and cavity-controlled modes,  $\bar{g}_h$ , for the optimized structural sensor location at (0.297 m, 0.360 m).

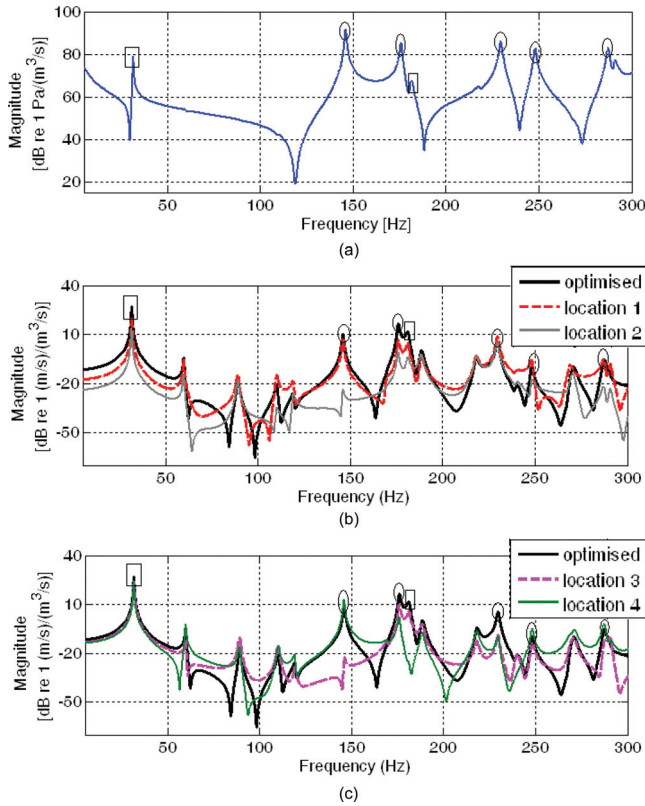


FIG. 10. (Color online) Frequency responses from an acoustic volume-velocity source at (0.430 m, 0.330 m, 0.850 m) to (a) acoustic pressure at the virtual sensor location (0.070 m, 0.816 m, 1.028 m), (b) velocity at structural sensor locations: optimized (0.297 m, 0.360 m), location 1 (0.173 m, 0.196 m), and location 2 (0.640 m, 0.300 m), and (c) velocity at structural sensor locations: optimized (0.297 m, 0.360 m), location 3 (0.510 m, 0.430 m), and location 4 (0.430 m, 0.730 m).  $\square$ : first and seventh panel-controlled modes,  $\odot$ : second to sixth cavity-controlled modes.

0.430 m), and location 4 (0.430 m, 0.730 m). The responses at the modes of interest vary depending on the sensor location. However, the optimized location provides the more consistent sensing performance over those modes. Structural sensor at location 3 had particularly low responses at the modes of interest, which impacted on the virtual sensing and active control performances as described in the following sections.

## B. Effects of structural sensor locations on virtual sensor and active control performances

The impact of structural sensor location on virtual sensor performance was investigated. The Kalman-filter based virtual sensor was used as a representative virtual sensor for performance analysis. This work considers the vibro-acoustic virtual sensor for active noise control proposed in Halim *et al.* (2011). A virtual sensor based on a nominal dynamic model was used, since the investigation was focused on the effect of sensor location to sensing performance. In this case, the robust vibro-acoustic virtual sensor design can be shown to converge to a standard Kalman-filter design. A discrete virtual sensor filter was implemented at the sampling frequency of 10 kHz. The primary disturbance was a volume-velocity source at (0.430 m, 0.330 m, 0.850 m) inside the cavity. The primary disturbance and structural measurement

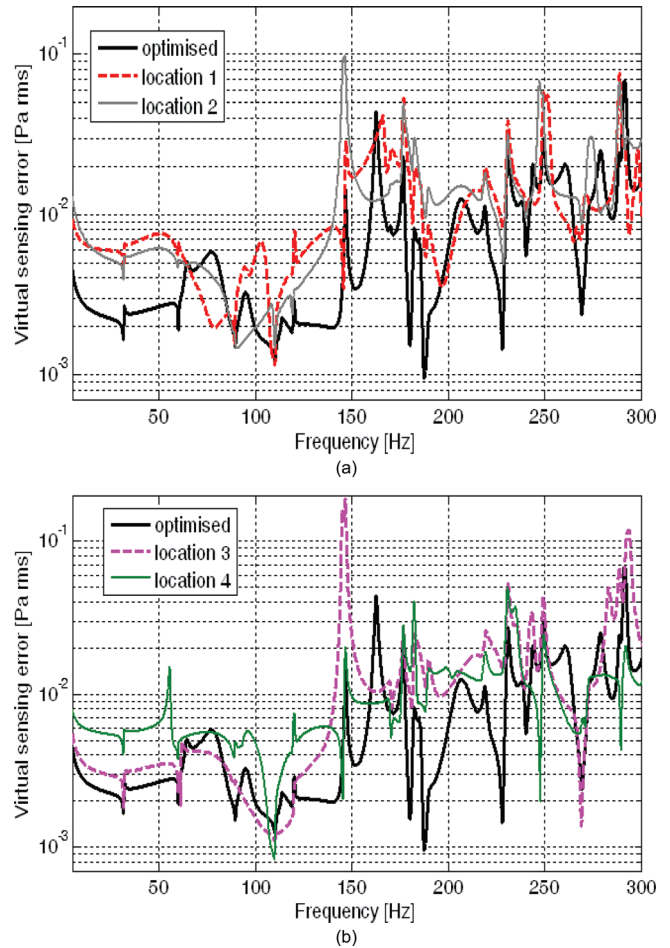


FIG. 11. (Color online) Virtual sensing error performance for virtual sensors designed using different structural sensor locations: (a) the optimized location (0.297 m, 0.360 m), location 1 (0.173 m, 0.196 m), and location 2 (0.640 m, 0.300 m), and (b) the optimized location (0.297 m, 0.360 m), location 3 (0.510 m, 0.430 m), and location 4 (0.430 m, 0.730 m).

noises have white-noise characteristics with discrete covariances of  $10^{-10} \text{ m}^6/\text{s}^2$  and  $10^{-14} \text{ m}^4/\text{s}^2$ , respectively. A volume-velocity secondary source was located at (0.520 m, 0.000 m, 0.240 m). The magnitude of the secondary control input was limited to 80% of the magnitude of primary disturbance.

For comparisons, virtual sensors are designed using structural sensors at different locations. In the implementation, the system's resonance frequencies were deliberately perturbed by +0.5% amounting to approximately 1.4 Hz for the sixth cavity-controlled mode. Figure 11 shows the 300 Hz-bandwidth virtual sensing error response. Over most frequencies, the "optimized" virtual sensor had generally lower virtual sensing error which was consistent with reasonably high modal observability levels aimed in the optimization as shown in Fig. 9. Using those virtual sensors, active tonal control was implemented and the control results are shown in Fig. 12, showing that the optimized virtual sensor achieved the superior control performance over the other virtual sensors. In particular, the dominant second to sixth cavity-controlled and first panel-controlled resonances had relatively high sound pressure attenuations. The effective control performance was expected because the virtual

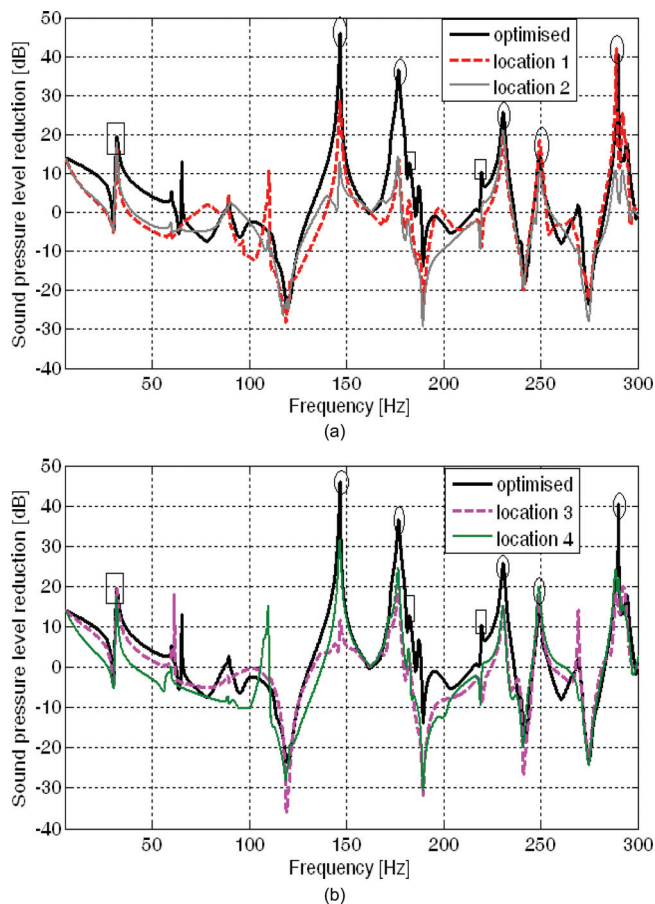


FIG. 12. (Color online) Noise reduction due to active control with virtual sensors designed using different structural sensor locations: (a) the optimized location (0.297 m, 0.360 m), location 1 (0.173 m, 0.196 m), and location 2 (0.640 m, 0.300 m), and (b) the optimized location (0.297 m, 0.360 m), location 3 (0.510 m, 0.430 m), and location 4 (0.430 m, 0.730 m). □: first, seventh, and ninth panel-controlled modes, ⊙: second to sixth cavity-controlled modes.

sensor was designed to minimize the broadband sensing error, mainly contributed by those modes as can be seen in Fig. 10(a). The virtual sensing error, relative to the true sound pressure, was small at those resonance regions, leading to a more accurate sound pressure estimation and consequently to a better active noise control performance. There was some noise increase in some frequency ranges such as in 60–130 Hz region, but those regions had already very low sound pressure responses at the anti-resonance regions [see Fig. 10(a)]. The control results indicate that high virtual sensing accuracy leads to high active control performance as expected, and the structural sensor location is a major factor in determining the virtual sensor performance.

## V. CONCLUSIONS

A structural sensor placement methodology for vibro-acoustic virtual sensor applications has been proposed. The virtual sensor aims to estimate the sound pressure inside an acoustic-structural coupled enclosure using solely structural sensors, without the use of acoustic sensors. Several conclusions were obtained from the work:

- (i) A spectral-spatially averaged performance metric has been proposed, which utilized the averaged structural sensor output energy of a vibro-acoustic system excited by a spatially varying point source. This vibro-acoustic performance metric was shown to be contributed by modal observability levels of panel- or cavity-controlled modes. The strength of each modal observability level was influenced by the modal coupling and resonance frequencies of associated uncoupled structural/cavity modes. The additive property of the spectral-spatially averaged performance metric allows modal contributions of panel- and cavity-controlled modes to be considered in a simple way for structural sensor placement.
- (ii) The effect of virtual sensor filter and disturbance/process and measurement noise to the virtual sensing error was studied. It was shown that the overall virtual sensing error energy was contributed additively by the modal virtual sensing error and the measurement noise energy. The modal virtual sensing error is contributed by the modal observability levels for the structural sensing and the target acoustic virtual sensing, which would influence the virtual sensor's filter gain.
- (iii) An optimization methodology was proposed for searching for the optimal sensor location with sufficiently high modal observability levels for certain important panel- and cavity-controlled modes. For an effective detection of a cavity-controlled mode, a structural sensor must be able to effectively observe multiple structural modes that are strongly coupled to that mode. The cavity-controlled modal observability measures were thus proposed to assist such a multiple-mode consideration in a simple but informative and intuitive way. Numerical study on a panel-cavity system demonstrated that a structural velocity sensor at the optimized location can be designed for effective detections and active control of acoustic-structural coupled modes, in particular for cavity-controlled modes.

## ACKNOWLEDGMENTS

The authors wish to acknowledge support given to them by the Research Grants Council of Hong Kong Special Administrative Region (HKSAR) through Grant No. PolyU 5132/07E.

- Cazzolato, B. S. (1999). "Sensing systems for active control of sound transmission in cavities," Ph.D. thesis, Adelaide University, South Australia, Chaps. 5–7, pp. 221–318.
- Cazzolato, B. (2002). "An adaptive LMS virtual microphone," in *Proceedings of Active 02*, Southampton, UK, pp. 105–116.
- Cheng, L. (1994). "Fluid structural coupling of a plate-ended cylindrical shell vibration and internal sound field," *J. Sound Vib.* **174**(5), 641–654.
- Cheng, L., and Nicolas, J. (1992). "Radiation of sound into a cylindrical enclosure from a point-driven end plate with general boundary conditions," *J. Acoust. Soc. Am.* **91**(3), 1504–1513.
- Elliott, S. J. (2001). *Signal Processing for Active Control* (Academic Press, San Diego, CA; London), Chaps. 2 and 4, pp. 49–102, 177–232.
- Elliott, S. J., and David, A. (1992). "A virtual microphone arrangement for local active sound control," in *Proceedings of First International Conference in Motion and Vibration Control*, Yokohama, Japan, pp. 1027–1031.

- Fahy, F. (1985) *Sound and Structural Vibration: Radiation, Transmission and Response* (Academic Press, London), Chap. 6, pp. 241–269.
- Gawronski, W. (1997). Actuator and sensor placement for structural testing and control,” *J. Sound Vib.* **208**(1), 101–109.
- Gawronski, W. (2004). *Advanced Structural Dynamics and Active Control of Structures* (Springer-Verlag, New York), Chaps. 4–5, pp. 65–141.
- Halim, D., Cheng, L., and Su, Z. (2011). “Virtual sensors for active noise control in acoustic-structural coupled enclosures using structural sensing: Optimization of structural sensor placement,” *J. Acoust. Soc. Am.* **129**(3), pp. 1390–1399.
- Halim, D., and Moheimani, S. O. R. (2003). “An optimization approach to optimal placement of collocated piezoelectric actuators and sensors on a thin plate,” *Mechatronics* **13**, 27–47.
- Hill, S. G., Tanaka, N., and Snyder, S. D. (2009). “A generalised approach for active control of structural-interior global noise,” *J. Sound Vib.* **326**(3–5), 456–475.
- Moheimani, S. O. R., Pota, H. R., and Petersen, I. R. (1999). “Spatial balanced model reduction for flexible structures,” *Automatica* **35**(2), 269–277.
- Moreau, D., Cazzolato, B. S., Zander, A. C., and Petersen, C. D. (2008). “A review of virtual sensing algorithm for active noise control,” *Algorithms* **1**, 69–99.
- Moreau, D., Ghan, J., Cazzolato, B. S., and Zander, A. (2009). “Active noise control in a pure tone diffuse sound field using virtual sensing,” *J. Acoust. Soc. Am.* **125**(6), 3742–3755.
- Pan, J., and Bies, D. A. (1990). “The effect of fluid—Structural coupling on sound waves in an enclosure—Theoretical part,” *J. Acoust. Soc. Am.* **87**(2), 692–707.
- Pawelczyk, M. (2003). “Multiple input-multiple output adaptive feedback control strategies for the active headrest system: Design and real-time implementation,” *Int. J. Adapt. Control Signal Process.* **17**(10), 785–800.
- Petersen, C. D., Fraanje, R., Cazzolato, B. S., Zander, A. C., and Hansen, C. H. (2008). “A Kalman filter approach to virtual sensing for active noise control,” *Mech. Syst. Signal Process.* **22**, 490–508.
- Popovich, S. (1997). Active acoustic control in remote regions, US Patent No. 5,701,350.
- Rafaely, B., Elliott, S., and Garcia-Bonito, J. (1999). “Broadband performance of an active headrest,” *J. Acoust. Soc. Am.* **106**(2), 787–793.
- Roure, A., and Albarrazin, A. (1999). “The remote microphone technique for active noise control,” in *Proceedings of Active 99*, Florida, USA, pp. 1233–1244.
- Smith, G. C., and Clark, R. L. (2001). “A crude method of loop-shaping adaptive structures through optimum spatial compensator design,” *J. Sound Vib.* **247**(3), 489–508.
- Snyder, S., and Tanaka, N. (1993). “On feedforward active control of sound and vibration using error signals,” *J. Acoust. Soc. Am.* **94**(4), 2181–2193.
- Zhou, K., Doyle, J. C., and Glover, K. (1996). *Robust and Optimal Control* (Prentice-Hall, Upper Saddle River), Chap. 4, pp. 91–116.